Dual-isometric Projected Entangled Pair States

Xie-Hang Yu,[1,2] J. Ignacio Cirac,[1,2] Pavel Kos,[1,2,*] and Georgios Styliaris[1,2,*]

[1]*Max-Planck-Institut für Quantenoptik, Hans-Kopfermann-Str. 1, 85748 Garching, Germany*
[2]*Munich Center for Quantum Science and Technology (MCQST), Schellingstr. 4, 80799 München, Germany*

Efficient characterization of higher dimensional many-body physical states presents significant challenges. In this paper, we propose a new class of Project Entangled Pair State (PEPS) that incorporates two isometric conditions. This new class facilitates the efficient calculation of general local observables and certain two-point correlation functions, which have been previously shown to be intractable for general PEPS, or PEPS with only a single isometric constraint. Despite incorporating two isometric conditions, our class preserves the rich physical structure while enhancing the analytical capabilities. It features a large set of tunable parameters, with only a subleading correction compared to that of general PEPS. Furthermore, we analytically demonstrate that this class can encode universal quantum computations and can represent a transition from topological to trivial order.

Introduction.—Efficiently representing strongly correlated many-body quantum states and extracting their relevant physical properties remains a pivotal challenge in dimensions higher than one. Tensor network methods offer an approach to address this problem. Following the successful application of 1D matrix product states (MPS) [1–3], Ref. [4] introduced their higher-dimensional generalization, projected entangled pair states (PEPS). These states satisfy an entanglement area law [5] and are considered a robust ansatz for representing ground states of gapped local Hamiltonians [6–14]. PEPS also play an important role in quantum dynamics [15–17], statistical mechanics [18–21], the classification of phases [22–25], and quantum machine learning [26–28].

Despite their advantages, finite PEPS still suffer from the rapid growth of the computational resources required for the calculation of physical quantities, such as expectation values of local observables, limiting the size of the system that can be investigated. In practice, even approximate algorithms on finite PEPS are costly and the errors are often hard to control [29–31]. This limitation also holds for translationally-invariant systems [32]. It has been shown that the exact contraction of a general PEPS is #P-hard [33], even for typical instances [34], which serves as a fundamental limitation.

One way to address this challenge is to consider some subclass of PEPS. One such class is the isometric PEPS (iso-PEPS) [35, 36], which extends the canonical form of 1D MPS to higher dimensions. Their isometric nature allows for the preparation of all iso-PEPS through sequential unitary circuits [37]. This sequential generation defines a time axis in the iso-PEPS and thus facilitates the backward contraction along this time direction [36]. Despite being typically short-range correlated [38], the iso-PEPS family can capture states with complex correlation, such as topological models and the associated phase transitions, which admit an exact representation within this class [39, 40].

However, the computation of the local observables for iso-PEPS is not always efficient. For example, an observable in the bulk of the tensor network may correspond to a later time expectation value in the associated sequential-circuit picture, which one expects to be intractable classically. Indeed, the computation of a local observable in 2D iso-PEPS is shown to
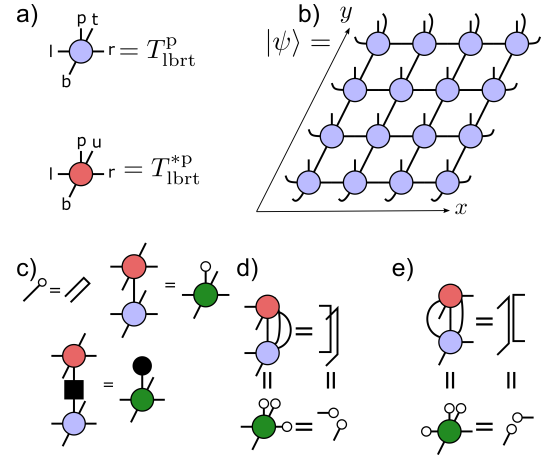
FIG. 1. a) Rank-5 tensor T of a PEPS. The complex conjugate of T is denoted by T^*. b) The physical state from the contracted local PEPS tensors, with the virtual space mapped to the physical one on the boundary. c) The local contraction of bra and ket PEPS states, with its folded notation shown on the right. The bottom panel shows the local expectation value of an observable (black square). The black dot on the right-hand side represents its vectorized form. d) Isometric condition in the unfolded and folded picture. e) Dual isometric condition.

be BQP-complete [41], which, subject to standard complexity theory assumptions, indicates that it is hard to simulate classically. Although in principle, some classical algorithms, like the Moses move [36, 42], can be used to approximate the result, the errors may remain uncontrolled [43]. This restricts the practical utility of the iso-PEPS and motivates the search for new classes of contractible PEPS.

In this letter, we introduce dual-isometric PEPS (DI-PEPS), a new subclass of iso-PEPS that enhances the computational tractability of tensor networks in higher dimensions, especially for computing local observables and certain two-point correlation functions. The class is defined by imposing an additional isometric condition onto iso-PEPS, which reduces the calculation of the above quantities in the 2D tensor network to a 1D tensor network. The latter is manageable and can be efficiently computed. More broadly, the dual-isometric

condition is analogous to dual-unitary gates [44], a class of exactly solvable quantum circuits, and can be seen as a natural extension of these ideas to PEPS. Furthermore, our work reveals that the DI-PEPS preserves the rich physical structure of iso-PEPS despite the additional constraint. For this, we show that DI-PEPS can encode universal quantum computations after post-selection. As a result, their output probability cannot be efficiently sampled on a classical computer. Additionally, by counting the number of free parameters of DI-PEPS, we show that this number is only reduced at subleading order as compared to conventional PEPS. Lastly, we develop a class of DI-PEPS which exhibits topological order and has a nontrivial transition to decoupled 1D chains. These findings underscore the DI-PEPS as a potent framework for investigating quantum many-body physics, offering new avenues for understanding and manipulating complex quantum systems.

PEPS and the folded picture.—We consider PEPS specified by a rank-5 tensor $T^{\mathrm{p}}_{\mathrm{lbrt}}$ for each vertex (x, y) of a 2D square lattice. The index p represents the physical degree of freedom with dimension d, and $\mathrm{l}, \mathrm{b}, \mathrm{r}, \mathrm{t}$ (left, bottom, right, top) label the virtual degrees of freedom, each χ-dimensional [Fig. (1a)]. Here $x \in \{1, \cdots, N\}$ and $y \in \{1, \cdots, M\}$. The wave function is obtained by locally contracting all the virtual degrees of freedom [Fig. (1b)]. At the boundary, the virtual space is isometrically mapped to the physical space; we explain this choice later. Thus, there are in total $(N + 2) \times (M + 2) - 4$ physical sites.

Our setting and results become more transparent via vectorizing; in graphical notation, this corresponds to "folding" [Fig. (1c)]. Given a fixed computational basis, an observable is vectorized to $\langle O|$ via $\sum_{ij} O_{ij} |i\rangle\langle j| \mapsto \sum_{ij} O_{ij} \langle i| \langle j|$. States are similarly mapped to a bipartite vector such that

$$\langle\psi|\hat{O}|\psi\rangle = \langle O|(|\psi^*\rangle \otimes |\psi\rangle). \tag{1}$$

Graphically, T^* is folded in front of T, thereby forming $T^* \otimes T = $ = .

Iso-PEPS.—Here we briefly review iso-PEPS [36], which is a subclass of PEPS satisfying the isometric condition

$$\sum_{\mathrm{r,t,p}} T^{\mathrm{p}}_{\mathrm{l_1 b_1 rt}} T^{*\mathrm{p}}_{\mathrm{l_2 b_2 rt}} = \delta_{\mathrm{l_1,l_2}}\delta_{\mathrm{b_1,b_2}}, \tag{2}$$

shown also graphically in Fig. (1d). This class can be understood as the 2D analog of the canonical form in MPS. Eq. (2) directly implies that iso-PEPS can be contracted starting from the top-right direction, until an observable is met [36].

Physically, every iso-PEPS tensor can be enlarged to a unitary

$$U^{\mathrm{prt}}_{\mathrm{lb}|0\rangle} = T^{\mathrm{p}}_{\mathrm{lbrt}} \tag{3}$$

with one of its inputs initialized to $|0\rangle$. This unitary gate also sequentially generates the corresponding state [37] in depth $\mathcal{O}(N+M)$. From this point of view, one can imagine that calculating expectation values of local observables in iso-PEPS

is as hard as quantum computation; indeed, this task was recently shown to be BQP-complete [41]. Note that the isometric property implies that only a local observable near the bottom/left boundary of the PEPS can be efficiently calculated [36], which corresponds to an operator along the light cone in a sequential quantum circuit. The latter only involves contribution from the boundary gates of a sequential quantum circuit as all of the bulk gates cancel with their hermitian conjugate [37].

Dual-isometric PEPS.—In this letter, we introduce a new subclass of iso-PEPS called dual-isometric PEPS (DI-PEPS). This is done by requiring another (dual) isometric condition

$$\sum_{\mathrm{l,t,p}} T^{\mathrm{p}}_{\mathrm{lb_1 r_1 t}} T^{*\mathrm{p}}_{\mathrm{lb_2 r_2 t}} = \delta_{\mathrm{r_1,r_2}}\delta_{\mathrm{b_1,b_2}}, \tag{4}$$

as shown in Fig. (1e). This is in analogy to dual-unitary circuits, where each gate can be interpreted as a valid evolution along a second "time" direction; DI-PEPS admit an additional sequential preparation direction.

The key point is that the dual condition, together with Eq. (2), allows an efficient calculation of expectation values of local observables. This becomes transparent in the folded picture, where this expectation value is expressed as

$$\langle\psi|O|\psi\rangle = \quad \text{} \tag{5}$$
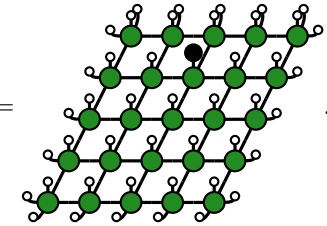
Starting from the top-left corner, we can use Eq. (4) [Fig. (1e)] to simplify the configuration as = . This procedure can be iterated, as now the same equation can be used in the next row and column. Following this simplification procedure, one finds that the dual-isometric condition Eq. (4) simplifies all of the diagram on the left side of the observable while the isometric condition Eq. (2) simplifies everything on the right side. As a consequence,
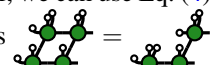
$$\langle\psi|O|\psi\rangle = \quad \text{} \tag{6}$$
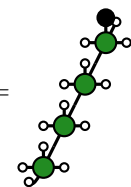
This is just a 1D tensor network, which can be efficiently contracted in $\mathcal{O}(M)$. This result also holds for local operators with support larger than 1. In that case, Eq. (6) includes more than one column but with constant (i.e., system-size independent) width.

Our next point of interest is two-point correlation functions, which play a key role in characterizing many-body properties.

They can be graphically expressed as

$$\langle\psi|O_1 O_2|\psi\rangle = \qquad\qquad . \qquad (7)$$

With the isometric and dual-isometric conditions, one can simplify the diagram from the top-left and top-right corners similarly as before. The final result is

$$\langle\psi|O_1 O_2|\psi\rangle = \qquad\qquad . \qquad (8)$$

Here we assume that the two operators are located at (x_1, y_1) and (x_2, y_2), respectively. The reduced 2D part of the tensor network is of size $t_1 \times t_2$, with $t_1 = |x_2 - x_1|$ and $t_2 = \min\{y_1, y_2\}$. If one of t_1 or t_2 is small enough, this contraction can be efficiently calculated using the linear transfer matrix within moderate resources. Specifically, if either t_1 or t_2 is constant, the correlator still reduces to a 1D tensor network with a possibly increased, but constant, bond dimension.

We investigate a generalization of the isometric conditions Eqs. (2) and (4) that preserves the solvability of 1- and 2-point correlations in [45].

Not only in our case, but also in general, the calculation of local or multi-point local expectation values in 2D PEPS can be interpreted as a circuit of 1+1D completely positive maps acting over the virtual space; in general, however, these are not trace-preserving. This is established by interpreting tensor-network diagrams, such as the one in Eq. (7), along a $45°$ counterclockwise rotated direction, and defining Kraus operators (indexed by p) as $E_{\mathrm{tr,lb}}^{\mathrm{p}} = T_{\mathrm{lbrt}}^{\mathrm{p}}$. Pictorially, this can be expressed as

$$l\,\substack{t\\\bullet\\b}\,r = \substack{t\quad r\\\blacksquare\\l\quad b}\,. \qquad (9)$$

where the right side depicts the completely positive map in the folded picture. For the case of iso-PEPS, this map is in addition trace-preserving, i.e., it corresponds to a valid quantum channel on the folded space. As such, it can be interpreted as a physical evolution. This evolution is in principle hard to compute, corresponding to the hardness of contracting PEPS in general. From this point of view, the solvability of DI-PEPS can be connected with the simplifying properties of two-unital space channels from Ref. [46].

The boundary condition of Fig. (1b) also obtains a physical interpretation at this stage. Viewing the PEPS as a quantum circuit, the boundary conditions correspond to initially preparing $N + M$ EPR-pairs, and inputting half of each pair to the circuit.

Examples of DI-PEPS.—As mentioned in Eq. (3), DI-PEPS can be prepared with a sequential quantum circuit with the additional condition $\sum_{\mathrm{ptl}} U_{\mathrm{lb_1}|0\rangle}^{\mathrm{pr_1 t}} (U_{\mathrm{lb_2}|0\rangle}^{\mathrm{pr_2 t}})^* = \delta_{\mathrm{b_1,b_2}} \delta_{\mathrm{r_1,r_2}}$, pictorially expressed as $=$. Some classes of unitary gates satisfying the above are:

Permutation-phase gates: $U = P_{231} D$ composed with arbitrary single site gates, where P_{231} is the shift-permutation $P_{231} = $ and D is an arbitrary diagonal gate in the computational basis. This family generalizes dual-unitary gates, for which P_{21} is just the SWAP [44], to a tripartite setting.

3-qubit gates ($d = \chi = 2$): We take a non-exhaustive ansatz $U = \prod_\alpha \exp(i Q_\alpha \sigma_2^\alpha \sigma_3^\alpha) \prod_\beta \exp(i J_\beta \sigma_1^\beta \sigma_2^\beta)$, where α, β run over $1, 2, 3$ and σ_m^α is the α Pauli matrix acting on the m-th qubit. We find that $Q_1 = 0, Q_2 = \pi/4, J_3 = \pi/4$ or $Q_2 = \pi/4, \cos 2J_1 \cos 2J_3 = \cos 2J_2 \cos 2Q_3 = 0$ and also simultaneous exchange of Q_1 and Q_2 as well as J_1 and J_2 all satisfy the condition. Moreover, additional arbitrary single site unitary on all five legs but the ancillary one associated with $|0\rangle$ are allowed.

Controlled-dual unitaries: $U_{\mathrm{lba}}^{\mathrm{prt}} = \sum_i |i\rangle_{\mathrm{p}} \langle i|_{\mathrm{a}} V_{\mathrm{tr,lb}}^i$, composed with arbitrary single site gates, where V^i is a dual-unitary gate [44], i.e., it is unitary and also satisfies $\sum_{\mathrm{tl}} V_{\mathrm{tr_1,lb_1}}^i V_{\mathrm{tr_2,lb_2}}^{*i} = \delta_{\mathrm{r_1,r_2}} \delta_{\mathrm{b_1,b_2}}$.

Next, we discuss another interesting example, which is not constructed from unitary gates, but from the *"plumbing tensor"* [40] which is a special PEPS with $D = \chi^4$. The local tensor $T_{\mathrm{lbrt}}^{\mathrm{p}}$ is determined by another rank-4 tensor W as

$$T_{\mathrm{lbrt}}^{\mathrm{p}} = T_{\mathrm{lbrt}}^{\mathrm{p_1 p_2 p_3 p_4}} = \delta_{\mathrm{l,p_1}} \delta_{\mathrm{b,p_2}} \delta_{\mathrm{r,p_3}} \delta_{\mathrm{t,p_4}} W_{\mathrm{lbrt}}, \qquad (10)$$

where $\mathrm{p}_i = 1, \ldots, \chi$. Graphically, $= $ with

$\perp$ denoting the delta tensor which is non-vanishing only if all three legs take the same value. The elements of the W matrix are restricted by Eqs. (2) and (4) (see [45] for its specific form). Now, if we place the W tensor at the vertices of a square lattice, the physical degrees of freedom lay on the edges[1]. Notably, the simplest case $\chi = 2$ includes the toric code tensor [40, 47] as an example of DI-PEPS. We will return to the topological properties of this class later.

Parameter counting and computational complexity.—Here we argue about the richness of DI-PEPS, despite them having analytically accessible correlation functions. As with every PEPS, the representation of the state in terms of tensors is nonunique. We take into account this so-called gauge freedom

---

[1] In fact, each edge hosts two spins but they are just a copy of each other and thus equivalent. One can merge these two spins into a single one by the transformation $\sum_{i=1}^\chi |i\rangle \langle ii|$.

by introducing a corresponding canonical form for the family of DI-PEPS that satisfies the generalized solvability conditions (see [45]). The resulting number of free real parameters of a normal[2] DI-PEPS (formed by repeating the same tensor) is $2(d-1)\chi^4$. Compared to the number of free real parameters $2d\chi^4 - 4\chi^2 + 2$ of a normal PEPS [45], we see that DI-PEPS covers a large subclass of normal PEPS.

We further consider the computational complexity of the DI-PEPS. Although one- and two-point correlators can be efficiently computed, we show that sampling of a DI-PEPS cannot be efficiently simulated in a classical computer. To this end, we demonstrate that the DI-PEPS can encode universal quantum computations with post-selection. Thus, according to Ref. [48], the output probability distribution cannot be sampled to a multiplicative precision by a classical computer efficiently, unless the polynomial hierarchy collapses to its third level, i.e., $\mathsf{postBQP} = \mathsf{postBPP}$.

While the proof is available in [45], here we sketch the main points. The idea is to encode dual-unitary quantum circuits in DI-PEPS and then utilize known results for their complexity [49]. Based on the previous discussion, we can interpret the PEPS as a 1+1D quantum circuit in the virtual (bond) space, while at the last layer the boundary bond outputs the computation result to physical space. We choose the DI-PEPS constructed from the controlled-dual-unitary gates (example above), where the physical index acts as the control. For each configuration of the measurement result, the evolution in the virtual space is then governed by a certain dual-unitary brick-wall quantum circuit. Importantly, the resulting dual-unitary circuit can simulate universal quantum computation after post-selection, which corresponds to measuring the physical state at the last layer of the DI-PEPS. The result then follows since, if a quantum state with post-selection can simulate universal quantum computation, the probability distribution cannot be sampled in polynomial time by a classical computer to a multiplicative precision unless $\mathsf{postBQP} = \mathsf{postBPP}$ [48].

DI-PEPS and topological states.—In this section, we consider in detail a $\chi = 2$ subfamily of the DI-PEPS constructed from the plumbing tensor of Eq. (10), with a special focus on its topological properties. To this end, we impose a $\mathbb{Z}_2$ symmetry on the W tensor

$$
-\!\boxed{W}\!- \; = \; -\!\sigma^3\!-\!\boxed{W}\!-\!\sigma^3\!- . \tag{11}
$$

This symmetry restricts its form to

$$
W_{\mathrm{lb,rt}} = \begin{pmatrix} \sqrt{\alpha} & & & \sqrt{1-\alpha} \\ & \sqrt{\beta} & \sqrt{1-\beta} & \\ & \sqrt{1-\alpha} & \sqrt{\alpha} & \\ \sqrt{1-\beta} & & & \sqrt{\beta} \end{pmatrix}, \tag{12}
$$

---

[2] A PEPS tensor is called normal if it becomes injective after blocking. Generic PEPS are normal [2].

with $\alpha, \beta \in [0,1]$, where we omit the complex phases of each element since they are irrelevant to the topological degeneracy.

Our aim is to probe the topological order of the above subfamily. Each PEPS is associated with a local parent Hamiltonian [2]. A PEPS is said to be in the topological order if the parent Hamiltonian has topological degeneracy of its ground states, which can be characterized by the transfer operator $\mathbb{T}$ [24, 50]. Parallel to Ref. [24], here we put the PEPS on a cylinder. We cut out one loop around the cylinder and contract it with its complex conjugate over the physical degrees to form the transfer operator in the doubled virtual space,

$$
\mathbb{T} = \;\vcenter{\hbox{\includegraphics{transfer}}}\; . \tag{13}
$$

According to the $\mathbb{Z}_2$ symmetry, the transfer operator can be block diagonalized into $\mathbb{T}_{p,\phi}^{p',\phi'}$, where p, p' denote the parity of the ket/bra state, respectively; $\phi, \phi' = 0, \pi$ denote whether a flux is threading the cylinder, i.e., if an additional σ^3 is present in the ket/bra virtual space. Due to the delta tensor in Eq. (10), we immediately see that $p = p'$ and the transformation $\phi(\phi') \to \phi(\phi') + \pi$ does not change the transfer operator. Thus, we only need to distinguish four transfer operators $\mathbb{T}_{\mathrm{e}\phi}^{\mathrm{e}\phi}, \mathbb{T}_{\mathrm{o}\phi}^{\mathrm{o}\phi}, \mathbb{T}_{\mathrm{e}\phi}^{\mathrm{e}\phi+\pi}, \mathbb{T}_{\mathrm{o}\phi}^{\mathrm{o}\phi+\pi}$.

The key point is that the leading eigenvalues $\lambda_{p\phi}^{p\phi'}$ and the corresponding degeneracy in each block determine the topological properties of the tensor. This is since they encode, in the thermodynamic limit, the inner product of the states corresponding to different choices of p, ϕ. Note that the latter may abruptly become linearly (in)dependent when tuning the parameters α, β, signaling a transition.

If $\alpha = \beta = \frac{1}{2}$, the resulting state is the toric code [40, 47], which has nontrivial topological order. At this point, $|\lambda_{\mathrm{e}\phi}^{\mathrm{e}\phi}| = |\lambda_{\mathrm{o}\phi}^{\mathrm{o}\phi}| = 1, |\lambda_{\mathrm{e}\phi}^{\mathrm{e}\phi+\pi}| = |\lambda_{\mathrm{o}\phi}^{\mathrm{o}\phi+\phi}| = 0$ and the blocks with the largest eigenvalues, $\mathbb{T}_{\mathrm{e}\phi}^{\mathrm{e}\phi}, \mathbb{T}_{\mathrm{o}\phi}^{\mathrm{o}\phi}$ are non-degenerate. The lines $\alpha = 1$ or $\beta = 1$, and the point $\alpha = \beta = 0$ are in the trivial phase, since they correspond to decoupled 1D chains, each in a GHZ state. Those points have exponentially many degeneracies in the leading eigenvalues of the transfer operators $\mathbb{T}_{\mathrm{e}\phi}^{\mathrm{e}\phi}, \mathbb{T}_{\mathrm{o}\phi}^{\mathrm{o}\phi}$ in the vertical dimension M and we refer to them as the GHZ-points. In the Supplemental Material [45], we moreover analytically show that except for the GHZ-points mentioned above, it always holds that $|\lambda_{\mathrm{e}\phi}^{\mathrm{e}\phi}| = |\lambda_{\mathrm{o}\phi}^{\mathrm{o}\phi}| > |\lambda_{\mathrm{e}\phi}^{\mathrm{e}\phi+\pi}| = |\lambda_{\mathrm{o}\phi}^{\mathrm{o}\phi+\phi}|$ and the blocks with the largest eigenvalues, $\mathbb{T}_{\mathrm{e}\phi}^{\mathrm{e}\phi}, \mathbb{T}_{\mathrm{o}\phi}^{\mathrm{o}\phi}$ are non-degenerate. We achieve that by mapping it to a frustration-free Hamiltonian. We also calculate the full spectrum of the transfer operators along the line $\alpha = \beta$ or $\alpha = 1 - \beta$ in [45]. Thus we can conclude that the DI-PEPS of Eq. (12) exhibit the same topological phase as the toric code, except from the GHZ-points. At those points we have a crossing from a topological phase which has degeneracy 4 to a decoupled phase with exponentially many degen-

eracies. This explicitly demonstrates that DI-PEPS contain topological phases.

Another important property of a PEPS is the locality of the parent Hamiltonian. In principle, the parent Hamiltonian can be obtained by blocking [2], which however may lead to terms with larger support. For example, if $d = \chi = 2$, generally it is sufficient to block 4×5 tensors and the resulting parent Hamiltonian is locally supported on these 20 sites. Numerically, this may be possible to improve by decomposing the resulting parent Hamiltonian into a sum of terms with smaller support, but it is very costly [51]. Our examples from Eq. (12) with non-vanishing α, β admit an analytical form of the parent Hamiltonians which are at most 8-local. In particular, if $\alpha = 1 - \beta$, this can be improved to a 4-local Hamiltonian. We illustrate the latter here while the general case follows a similar argument [45]. The state with $\alpha = 1 - \beta$ can be obtained by acting with a single-body operator $\mathcal{U}_v = e^{s\sigma^3}$ on each vertical edge of the toric code, with $s = \frac{1}{4} \ln \frac{\alpha}{1-\alpha}$. The toric code has the well-known parent Hamiltonian $H_{\text{TC}} = \sum h_{\text{TC}}$ with each h_{TC} 4-local [47]. The parent Hamiltonian of our states H is thus connected to that of toric code as $H = \sum h$ with

$$ h = \prod_v \mathcal{U}_v^{-1\dagger} h_{\text{TC}} \mathcal{U}_v^{-1}. \tag{14} $$

Here v belongs to the vertical edges which overlap with h_{TC}. The above transformation does not change the locality of h which remains 4.

Discussion and outlook.— In this letter, we proposed a new class of PEPS called DI-PEPS, with two isometric conditions. This PEPS allows for efficient computational of local and certain two-point correlation functions. Furthermore, we have shown that this class exhibits interesting physical properties. It has a large number of free parameters, encodes universal quantum computation after post-selection and can represent interesting transitions from topological to trivial order.

Let us now discuss possible generalizations. First of all, we can impose further isometric conditions, from bottom-left and (or) bottom-right. In this case, higher-point correlation functions are also tractable. One can figure out that for a PEPS with n-isometric conditions, all the $(n-1)$-point correlation functions are solvable. For example, if we consider a 4-isometric PEPS, all the three-point correlation functions can be reduced to a 1D tensor network. Although in our study we focus on the 2D square lattice, the generalization to higher dimensions or different lattices is also interesting. We may consider the 3D simple cubic lattice, or the triangle lattice where one can define up to six isometric conditions. Another further direction is to go beyond correlation functions and investigate other quantities, such as the entanglement entropy.

Lastly, the equivalence between PEPS and 1+1D quantum dynamical completely-positive maps may guide us to construct new classes of solvable local quantum evolutions for any solvable PEPS. As an example, we look at Sequentially Generated States (SGS) [52], which satisfy

$$ \text{} \tag{15} $$

We can use our proposed duality to define a new kind of solvable quantum map with the property

$$ \text{} \tag{16} $$

This class allows the efficient calculation of local and two-point expectation values, as it can decouple different layers along the diagonal line. A somehow related unitary example was recently proposed in [53]. Importantly, this class is solvable even for non-trace preserving dynamics, like for measurement-induced phase transitions.

* These authors contributed equally.
[1] M. Fannes, B. Nachtergaele, and R. F. Werner, Finitely correlated states on quantum spin chains, Communications in mathematical physics **144**, 443 (1992).
[2] J. I. Cirac, D. Pérez-García, N. Schuch, and F. Verstraete, Matrix product states and projected entangled pair states: Concepts, symmetries, theorems, Rev. Mod. Phys. **93**, 045003 (2021).
[3] J. Haegeman and F. Verstraete, Diagonalizing transfer matrices and matrix product operators: A medley of exact and computational methods, Annual Review of Condensed Matter Physics **8**, 355–406 (2017).
[4] F. Verstraete and J. I. Cirac, Renormalization algorithms for quantum-many body systems in two and higher dimensions (2004), arXiv:cond-mat/0407066 [cond-mat.str-el].
[5] J. Eisert, M. Cramer, and M. B. Plenio, Colloquium: Area laws for the entanglement entropy, Rev. Mod. Phys. **82**, 277 (2010).
[6] H. Niggemann, A. Klümper, and J. Zittartz, Quantum phase transition in spin-3/2 systems on the hexagonal lattice—optimum ground state approach, Zeitschrift für Physik B Condensed Matter **104**, 103 (1997).
[7] F. Verstraete and J. I. Cirac, Matrix product states represent ground states faithfully, Phys. Rev. B **73**, 094423 (2006).
[8] F. Verstraete, M. M. Wolf, D. Perez-Garcia, and J. I. Cirac, Criticality, the area law, and the computational power of projected entangled pair states, Phys. Rev. Lett. **96**, 220601 (2006).
[9] M. B. Hastings, An area law for one-dimensional quantum systems, Journal of statistical mechanics: Theory and experiment **2007**, P08024 (2007).
[10] F. G. Brandao and M. Horodecki, Exponential decay of correlations implies area law, Communications in mathematical physics **333**, 761 (2015).
[11] A. Molnar, N. Schuch, F. Verstraete, and J. I. Cirac, Approximating Gibbs states of local Hamiltonians efficiently with projected entangled pair states, Physical review B **91**, 045138 (2015).

[12] A. Anshu, A. W. Harrow, and M. Soleimanifar, Entanglement spread area law in gapped ground states, Nature Physics **18**, 1362–1366 (2022).

[13] A. Anshu, I. Arad, and D. Gosset, An area law for 2d frustration-free spin systems, in *Proceedings of the 54th Annual ACM SIGACT Symposium on Theory of Computing* (2022) pp. 12–18.

[14] M. J. O'Rourke and G. K.-L. Chan, Entanglement in the quantum phases of an unfrustrated Rydberg atom array, Nature Communications **14**, 5397 (2023).

[15] I. Pižorn, L. Wang, and F. Verstraete, Time evolution of projected entangled pair states in the single-layer picture, Physical Review A **83**, 052321 (2011).

[16] R. T. Ponnaganti, M. Mambrini, and D. Poilblanc, Real-time dynamics of a critical resonating valence bond spin liquid, Phys. Rev. B **106**, 195132 (2022).

[17] R. T. Ponnaganti, M. Mambrini, and D. Poilblanc, Tensor network variational optimizations for real-time dynamics: Application to the time-evolution of spin liquids, SciPost Phys. **15**, 158 (2023).

[18] M. Levin and C. P. Nave, Tensor renormalization group approach to two-dimensional classical lattice models, Phys. Rev. Lett. **99**, 120601 (2007).

[19] Z. Y. Xie, H. C. Jiang, Q. N. Chen, Z. Y. Weng, and T. Xiang, Second renormalization of tensor-network states, Phys. Rev. Lett. **103**, 160601 (2009).

[20] H. H. Zhao, Z. Y. Xie, Q. N. Chen, Z. C. Wei, J. W. Cai, and T. Xiang, Renormalization of tensor-network states, Phys. Rev. B **81**, 174411 (2010).

[21] H.-H. Zhao, Z.-Y. Xie, T. Xiang, and M. Imada, Tensor network algorithm by coarse-graining tensor renormalization on finite periodic lattices, Phys. Rev. B **93**, 125115 (2016).

[22] X. Chen, Z.-C. Gu, and X.-G. Wen, Classification of gapped symmetric phases in one-dimensional spin systems, Phys. Rev. B **83**, 035107 (2011).

[23] N. Schuch, D. Pérez-García, and I. Cirac, Classifying quantum phases using matrix product states and projected entangled pair states, Phys. Rev. B **84**, 165139 (2011).

[24] N. Schuch, D. Poilblanc, J. I. Cirac, and D. Pérez-García, Topological order in the projected entangled-pair states formalism: Transfer operator and boundary Hamiltonians, Phys. Rev. Lett. **111**, 090501 (2013).

[25] P. Corboz, P. Czarnik, G. Kapteijns, and L. Tagliacozzo, Finite correlation length scaling with infinite projected entangled-pair states, Phys. Rev. X **8**, 031031 (2018).

[26] Z. Liu, Q. Ye, L.-W. Yu, L. M. Duan, and D.-L. Deng, Theory on variational high-dimensional tensor networks (2023), arXiv:2303.17452 [quant-ph].

[27] S. Cheng, L. Wang, and P. Zhang, Supervised learning with projected entangled pair states, Phys. Rev. B **103**, 125117 (2021).

[28] A. Azizi, K. Najafi, and M. Mohseni, Learning phase transition in Ising model with tensor-network Born machines (2020).

[29] M. Lubasch, J. I. Cirac, and M.-C. Bañuls, Algorithms for finite projected entangled pair states, Phys. Rev. B **90**, 064425 (2014).

[30] M. Lubasch, J. I. Cirac, and M.-C. Bañuls, Unifying projected entangled pair state contractions, New Journal of Physics **16**, 033014 (2014).

[31] G. Scarpa, A. Molnár, Y. Ge, J. J. García-Ripoll, N. Schuch, D. Pérez-García, and S. Iblisdir, Projected entangled pair states: Fundamental analytical and numerical limitations, Phys. Rev. Lett. **125**, 210504 (2020).

[32] L. Vanderstraeten, J. Haegeman, P. Corboz, and F. Verstraete, Gradient methods for variational optimization of projected entangled-pair states, Physical Review B **94**, 155123 (2016).

[33] N. Schuch, M. M. Wolf, F. Verstraete, and J. I. Cirac, Computational complexity of projected entangled pair states, Phys. Rev. Lett. **98**, 140506 (2007).

[34] J. Haferkamp, D. Hangleiter, J. Eisert, and M. Gluza, Contracting projected entangled pair states is average-case hard, Phys. Rev. Res. **2**, 013010 (2020).

[35] R. Haghshenas, M. J. O'Rourke, and G. K.-L. Chan, Conversion of projected entangled pair states into a canonical form, Physical Review B **100**, 054404 (2019).

[36] M. P. Zaletel and F. Pollmann, Isometric tensor network states in two dimensions, Phys. Rev. Lett. **124**, 037201 (2020).

[37] Z.-Y. Wei, D. Malz, and J. I. Cirac, Sequential generation of projected entangled-pair states, Phys. Rev. Lett. **128**, 010607 (2022).

[38] D. Haag, F. Baccari, and G. Styliaris, Typical correlation length of sequentially generated tensor network states, PRX Quantum **4**, 030330 (2023).

[39] T. Soejima, K. Siva, N. Bultinck, S. Chatterjee, F. Pollmann, and M. P. Zaletel, Isometric tensor network representation of string-net liquids, Phys. Rev. B **101**, 085117 (2020).

[40] Y.-J. Liu, K. Shtengel, and F. Pollmann, Topological quantum phase transitions in 2d isometric tensor networks (2024), arXiv:2312.05079 [quant-ph].

[41] D. Malz and R. Trivedi, Computational complexity of isometric tensor network states (2024), arXiv:2402.07975 [quant-ph].

[42] Y. Wu, S. Anand, S.-H. Lin, F. Pollmann, and M. P. Zaletel, Two-dimensional isometric tensor networks on an infinite strip, Phys. Rev. B **107**, 245118 (2023).

[43] S.-H. Lin, M. P. Zaletel, and F. Pollmann, Efficient simulation of dynamics in two-dimensional quantum spin systems with isometric tensor networks, Phys. Rev. B **106**, 245102 (2022).

[44] B. Bertini, P. Kos, and T. Prosen, Exact correlation functions for dual-unitary lattice models in 1+ 1 dimensions, Physical review letters **123**, 210601 (2019).

[45] See the Supplemental Material for details.

[46] P. Kos and G. Styliaris, Circuits of space and time quantum channels, Quantum **7**, 1020 (2023).

[47] A. Y. Kitaev, Fault-tolerant quantum computation by anyons, Ann. Phys. **303**, 2 (2003).

[48] M. J. Bremner, R. Jozsa, and D. J. Shepherd, Classical simulation of commuting quantum computations implies collapse of the polynomial hierarchy, Proceedings of the Royal Society A: Mathematical, Physical and Engineering Sciences **467**, 459 (2011).

[49] R. Suzuki, K. Mitarai, and K. Fujii, Computational power of one- and two-dimensional dual-unitary quantum circuits, Quantum **6**, 631 (2022).

[50] N. Schuch, I. Cirac, and D. Pérez-García, Peps as ground states: Degeneracy and topology, Annals of Physics **325**, 2153 (2010).

[51] G. Giudici, J. I. Cirac, and N. Schuch, Locality optimization for parent Hamiltonians of tensor networks, Phys. Rev. B **106**, 035109 (2022).

[52] M. C. Bañuls, D. Pérez-García, M. M. Wolf, F. Verstraete, and J. I. Cirac, Sequentially generated states for the study of two-dimensional systems, Phys. Rev. A **77**, 052306 (2008).

[53] H.-R. Wang, X.-Y. Yang, and Z. Wang, Exact Markovian dynamics in quantum circuits (2024), arXiv:2403.14807 [quant-ph].

[54] R. Raussendorf, D. E. Browne, and H. J. Briegel, Measurement-based quantum computation on cluster states, Phys. Rev. A **68**, 022312 (2003).

[55] M. A. Nielsen and I. Chuang, *Quantum computation and quantum information* (Cambridge University Press, 2002).

[56] D. Pérez-García, M. Sanz, C. Gonzalez-Guillen, M. M. Wolf,

and J. I. Cirac, Characterizing symmetries in a projected entangled pair state, New Journal of Physics **12**, 025010 (2010).

[57] A. Molnar, J. Garre-Rubio, D. Pérez-García, N. Schuch, and J. I. Cirac, Normal projected entangled pair states generating the same state, New Journal of Physics **20**, 113017 (2018).

[58] L. Piroli, B. Bertini, J. I. Cirac, and T. Prosen, Exact dynamics in dual-unitary quantum circuits, Phys. Rev. B **101**, 094304 (2020).

APPENDIX

1. Computational complexity

In this subsection, we investigate the computational complexity of DI-PEPS. We will demonstrate that, with postselection, DI-PEPS can simulate universal quantum computations. Thus the output probability distribution cannot be sampled to a multiplicative precision by a classical computer efficiently unless the Polynomial Hierarchy collapses to its third level, i.e., $\mathsf{postBQP} = \mathsf{postBPP}$ [48]. We prove this by encoding dual-unitary quantum circuits into the DI-PEPS and referring to known results on their complexity [49].

We consider the following DI-PEPS with the same boundary condition as in Fig. (1b) of the main text

$$\text{(S1)}$$
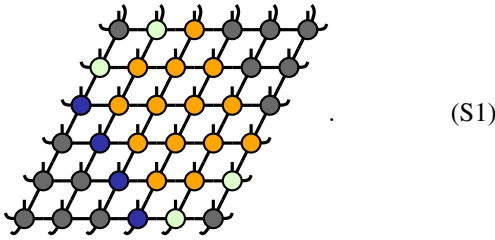
Here we use four different kinds of local tensors, denoted by their colors. From the explicit construction shown below, one can verify that all of them satisfy the condition of DI-PEPS. We choose physical dimension $d = 16$ and virtual dimension $\chi = 2$. However, locally the tensor can have an effective physical dimension[3] lower than 16, denoted as d_e, as only a subspace of the larger physical Hilbert space is relevant.

Orange tensor: It is a special case of the class "controlled-dual unitaries" proposed in the main text, but with $d_e = 1$, i.e.,

$$T^{\mathrm{p}}_{\mathrm{lbrt}} = \delta_{\mathrm{p},1} V_{\mathrm{tr,lb}}. \tag{S2}$$

Here V is dual unitary [44]. This tensor can be interpreted as a 1+1D quantum circuit composed of dual-unitary gates acting over the virtual space from left-bottom to right-top. This tensor is the main ingredient for providing the computational complexity of DI-PEPS.

---

[3] I.e., the dimension of the image of the tensor, when viewed as a map from virtual to physical space.

Light-green tensor: This tensor with $d_e = 16$ is composed of a bipartite physical space, each with dimension 4, such that

$$T^{\mathrm{p_1 p_2}}_{\mathrm{lbrt}} = \langle \mathrm{lt}|\phi^{p_1}\rangle \langle \mathrm{rb}|\phi^{p_2}\rangle. \tag{S3}$$

Here $|\phi^{p_{1(2)}}\rangle$ with $p_{1(2)} \in \{1, 2, 3, 4\}$ are the four Bell basis states $|\phi^1\rangle = \frac{|00\rangle + |11\rangle}{\sqrt{2}}$, $|\phi^2\rangle = \frac{|00\rangle - |11\rangle}{\sqrt{2}}$, $|\phi^3\rangle = \frac{|01\rangle + |10\rangle}{\sqrt{2}}$, $|\phi^4\rangle = \frac{|01\rangle - |10\rangle}{\sqrt{2}}$. The state $|\phi^1\rangle$ is also called an EPR pair. The light-green tensor serves as the boundary condition of the dual-unitary circuit. For those on the left-top, we post-select the measurement outcome to $p_2 = 1$ and on the right-bottom, we post-select the output to $p_1 = 1$ such that the boundary condition for the dual-unitary circuit is

$$\text{(S4)}$$
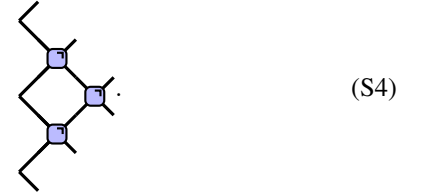
where the blue rectangles are some dual-unitary gates, following the same notation as in [44]. Thus, the dynamic in the virtual space is driven by a dual-unitary quantum circuit.

Dark-blue tensor: This tensor with $d_e = 4$ is defined as

$$T^{\mathrm{p}}_{\mathrm{lbrt}} = U^{\mathrm{p}}_{\mathrm{lb}} \langle \mathrm{rt}|\phi^1\rangle. \tag{S5}$$

Here U is an isometry from the left-bottom virtual spaces to physical space, and $|\phi^1\rangle$ corresponds to an EPR pair of the right-top virtual space of the dark-blue tensor. The dark-blue tensors together prepare a chain of EPR pairs that serve as the initial state for the dual-unitary circuit dynamics in the virtual space. The dark-blue tensors also effectively decouple the left-bottom space from the right-top space.

Grey tensor: This tensor with $d_e = 1$ is defined as

$$T^{\mathrm{p}}_{\mathrm{lbrt}} = \delta_{\mathrm{p},1}\delta_{\mathrm{l,r}}\delta_{\mathrm{b,t}}. \tag{S6}$$

This grey tensor is just the SWAP gate in virtual bonds as can be seen in Eq. (9). Pictorially this can be viewed as

$$\text{(S7)}$$

The information of state is thus swapped to the boundary which is finally read out.

Therefore, with the above choices, the resulting DI-PEPS can be interpreted as a 1+1D dual-unitary quantum circuit (orange PEPS) over the virtual space with a chain of EPR pairs as the initial state (dark-blue PEPS). The output of this circuit is transmitted to the top-right boundary, which is further transmitted to the physical space and "read out" by the last layer of the PEPS. From Ref. [49], a dual-unitary quantum circuit with initial state a chain of EPR pairs can prepare the cluster state,

which serves as the well-known measurement-based universal quantum computation [54]. Thus, DI-PEPS under postselection can simulate universal quantum computation. According to Ref. [48], quantum states which can encode postselected quantum computation are unlikely to be classically samplable to multiplicative precision, unless postBQP = postBPP.

2. Dimension of the DI-PEPS manifold, generalized families, and canonical form

In this subsection, we explore some mathematical properties of DI-PEPS and their generalization. We discuss the dimension of the underlying manifold and a canonical form. The number of free parameters here always refers to the real degrees of freedom.

$$\text{(S9)}$$

Here — denotes an element in the space orthogonal to $|\!\!-\!\!\circ\rangle$. This space is thus spanned by (vectorized) traceless Hermitian matrices which have $\chi^2 - 1$ free parameters.

The subscript of a follows the usual order left, bottom, right, top. Therefore the DI-PEPS condition amounts to $a_{\circ\circ\circ\circ} = 1$ and $a_{-\circ\circ\circ} = a_{--\circ\circ} = a_{\circ-\circ\circ} = a_{\circ\circ-\circ} = a_{\circ--\circ} = 0$ with no restriction on the other components. Thus the space of quantum channels corresponding to DI-PEPS forms a convex subset in the space of completely positive and trace-preserving maps (i.e., quantum channels) with dimension $\chi^8 - 2\chi^4 + \chi^2$. Here the additional requirement that the corresponding channel should be a completely positive map does not change the above parameter counting [46].

To obtain the number of free parameters of the original PEPS $T^{\mathrm{p}}_{\mathrm{lbrt}}$, we need to consider the freedom in the physical index p, which corresponds to the Kraus index in the corresponding representation of a quantum channel. Recall that two Kraus representations are equivalent if and only if they are related by an isometry [55]. In our case, we can select an (arbitrary) set of Kraus operator, $\widetilde{E}^{\mathrm{i}}_{\mathrm{tr,lb}}$ with $i \in \{1, \cdots, \chi^4\}$, to represent the channel corresponding to the contracted DI-PEPS. The original PEPS is thus expressed as $T^{\mathrm{p}}_{\mathrm{lbrt}} = \sum_{\mathrm{i}} V_{\mathrm{pi}} \widetilde{E}^{\mathrm{i}}_{\mathrm{tr,lb}}$. Here V satisfies $V^\dagger V = I_{\chi^4}$ with $2d\chi^4 - \chi^8$ free parameters. Since here we assume the ten-

a. Dimension of the DI-PEPS manifold

We first consider the injective PEPS, which is a generic case for $d \geq \chi^4$. Recall that a PEPS tensor is called injective if the corresponding map from virtual to physical space is injective [2]. In order to calculate the dimension of the manifold, we recall that a folded PEPS, after contracting the physical degrees of freedom, can be viewed as a completely positive map, shown in Eq. (9). The number of free parameters of completely positive maps corresponding to DI-PEPS is then equal to the one of the two-unital channels in Ref. [46]. The latter can be obtained by perturbing around the totally depolarizing channel [46]. For completeness, we repeat this analysis here.

We denote the (conveniently normalized) vectorized identity operator as

$$|\!\!-\!\!\circ\rangle = \begin{cases} \sum_i |ii\rangle & \text{on physical space} \\ \frac{1}{\sqrt{\chi}} \sum_i |ii\rangle & \text{on virtual space} \end{cases}, \quad \text{(S8)}$$

where χ is the dimension of the virtual space. With this notation, the decomposition of a contracted PEPS over the doubled space can be schematically expressed as

sor to be injective, $\widetilde{E}^{\mathrm{i}}_{\mathrm{tr,lb}}$ are linearly independent and thus different isometries V must lead to different tensors T. The total number of free parameters of injective DI-PEPS is thus

$$2d\chi^4 - \chi^8 + \chi^8 - 2\chi^4 + \chi^2 = 2(d-1)\chi^4 + \chi^2. \quad \text{(S10)}$$

For non-injective tensors, it is possible that different isometries lead to the same tensor, so the above counting does not apply directly. Nevertheless, we have numerically calculated the dimension of the tangent space of DI-PEPS and found that Eq. (S10) holds for generic (non-injective) PEPS for $d < \chi^4$. A notable exception is the permutation-phase gates of the main text [also in Eq. (S7)], which have a larger tangent space dimension.

In fact, the following intuitive argument suggests that Eq. (S10) serves as a lower bound for the number of free parameters. A general PEPS has $2d\chi^4$ free parameters. The isometric condition Eq. (2) imposes χ^4 constraints and the dual isometric condition Eq. (4) imposes another χ^4 constraints. However, these constraints are not linearly independent since both Eqs. (2) and (4) require that = , which includes χ^2 equations. Therefore the number of linearly constraint equations is at most $2\chi^4 - \chi^2$. The free parameters are thus, at least, $2d\chi^4 - 2\chi^4 + \chi^2$.

Note that, so far, we have focused on counting parameters that specify a local tensor and not a physical state. We address this in the following, after first introducing more general isometric conditions.

b. Generalized families and canonical form

The constraints of Eqs. (2) and (4) for a PEPS are not the most general ones allowing the efficient calculation of expectation values using our strategy. A more general definition of a solvable PEPS may be written as

$$\sum_{r,t,r',t',p} T^{p}_{l_1 b_1 r t} S_{r,r'} R_{t,t'} T^{*p}_{l_2 b_2 r' t'} = S_{l_1,l_2} R_{b_1,b_2}, \quad (S11)$$

$$\sum_{l,t,l',t',p} T^{p}_{l b_1 r_1 t} B_{l,l'} R_{t,t'} T^{*p}_{l' b_2 r_2 t'} = B_{r_1,r_2} R_{b_1,b_2}. \quad (S12)$$

Here S, R, B are arbitrary matrices. Graphically, this can be expressed as

$$(S13)$$

$$(S14)$$

Here we use $\diamondsuit, \triangle, \square$ to represent the vectorized S, R, B matrices, respectively.

We choose open boundary conditions described by rank-4 tensors (rank-3 at the corners). The requirement for solvability over those boundary tensors will be discussed in the next subsection. Here we only focus on the bulk tensor, which is assumed to be translationally invariant for simplicity, and consider its degrees of freedom.

Although two PEPS tensors may be different, the resulting states may be the same; this is known as gauge freedom [2]. We now use this freedom to bring the matrices S, R, B into a canonical form. In the following, we restrict our discussion to normal PEPS [2]. For this class, the gauge freedom is well-understood [56] (including for open boundary conditions [57]). In particular, two normal tensors represent the same state if and only if they can be connected by a gauge transformation

$$(S15)$$

(see Ref. [57]), with Q, J arbitrary invertible matrices. After the gauge transformation, the corresponding eigenvectors S, R, B in Eqs. (S11) and (S12) will also be changed. In the following, we use this gauge freedom to bring the matrices S, R, B into a canonical form.

A normal PEPS can be blocked into a large rectangle tensor such that it is injective. The blocked region is depicted as

$$(S16)$$

The corresponding folded tensor after contracting the physical degrees then defines a completely positive map, when interpreted from top-right to bottom-left. We recognize that

$$(S17)$$

is an eigenvector with the eigenvalue 1. We assume that this map has no eigenvalue larger than 1 for a large enough blocking, which will be justified in the next paragraph. Since this blocked tensor is injective, we can use a lemma from [58] which states that the completely positive map corresponding to an injective tensor is primitive and thus its leading eigenvector must be unique and strictly positive definite. This implies that the matrices S, R are strictly positive definite. Parallel to Ref. [58], we choose $J = R^{\frac{1}{2}}$ and $Q = S^{-\frac{1}{2}}$ such that for the new tensor $\widetilde{T}$, Eq. (S11) reduces to the isometric condition Eq. (2) and Eq. (S12) simplifies to a new one with R replaced by the identity matrix and B replaced by $\widetilde{B} = S^{\frac{1}{2}} B S^{\frac{1}{2}}$.

Here we argue that the assumption that the map after large enough blocking has no eigenvalue larger than 1 is sensible. To this end, we require without loss of generality that the state is normalized in the thermodynamic limit. Equation (S16) is further blocked horizontally and then vertically to form a corner transfer operator [32], i.e., the basic tensor of the corner transfer operator is now replaced by the blocked one of Eq. (S16). According to Ref. [32], the norm of the state can be approximated by the power of the leading eigenvalue of the corner transfer operator, which suggests that no eigenvalue larger than 1 is allowed as long as the state is normalized in the thermodynamic limit. For the corner transfer operator constructed above, Eq. (S17) with extension to infinity is just the eigenvector with eigenvalue 1, which means that it is the leading eigenvector. Since the corner transfer operator is formed by folding an injective tensor [constructed from Eq. (S16)], we immediately obtain that S, R are strictly positive definite [58] and everything else follows as before.

Now, the only gauge freedom remaining which does not change Eq. (2) is the unitary gauge, i.e., we can choose J, Q to be both unitary. Since the matrix $\widetilde{B}$ is positive definite (following a similar argument), this gauge choice can be used to diagonalize it. For simplicity, we assume that the eigenbasis of $\widetilde{B}$ is non-degenerate, which is the generic case. Thus, the canonical form of the solvable PEPS can be expressed as

(here we use the symbol T to also represent the tensor after the gauge transformations from above were implemented)

$$\sum_{r,t,p} T^{\mathrm{p}}_{l_1 b_1 rt} T^{*\mathrm{p}}_{l_2 b_2 rt} = \delta_{l_1,l_2}\delta_{b_1,b_2}, \qquad (S18)$$

$$\sum_{l,t,p} T^{\mathrm{p}}_{l b_1 r_1 t}\Lambda_{l,l} T^{*\mathrm{p}}_{l b_2 r_2 t} = \Lambda_{r_1,r_1}\delta_{r_1,r_2}\delta_{b_1,b_2} \qquad (S19)$$

for some diagonal matrix Λ. Or equivalently in graphical notation

$$(S20)$$

$$(S21)$$

with the white square now the vectorized form of Λ. At this stage, the remaining gauge corresponds to Q being the diagonal phase matrix in the same eigenbasis as Λ, and J being any unitary matrix.

The number of free parameters associated with the physical state described by a uniform solvable normal PEPS [i.e., satisfying Eqs. (S13) and (S14)] can be estimated from the free parameters of the canonical form [Eqs. (S20) and (S21)] minus the remaining gauge. Eq. (S19) or (S21) with any fixed diagonal matrix Λ allows a similar decomposition as in Eq. (S9). We just need to replace the right empty bullet $\circ\!\!-$ in Eq. (S9) with $\square\!\!-$ (vectorized Λ), and also the left solid line in Eq. (S9) with an element in the orthogonal space of Λ. This corresponds to the biorthogonal decomposition in the horizontal direction where the left and right eigenvectors are different. For example, the first term would be $-\!\!\circ\!\!\square\!\!-$. Thus, for any fixed Λ, a generic PEPS satisfying Eqs. (S18), (S19) has the same number of free parameters as the one satisfying Eqs. (2), (4), but with Λ contributing additional $\chi - 1$ free parameters (here we have subtracted the global scaling $\Lambda \to c\Lambda$ with c a constant).

Combining all the things together, we arrive at the total number of free parameters associated with the generic physical state (i.e., the one satisfying all previous assumptions) as

$$2(d-1)\chi^4 + \chi^2 + \chi - 1 - (\chi - 1 + \chi^2 - 1) - 1$$
$$=2(d-1)\chi^4. \qquad (S22)$$

Here the term in the second parenthesis represents the gauge freedom of J, Q (whose global phase is irrelevant since it cancels with J^{-1}, Q^{-1}). The last -1 comes from the fact that two tensors T differing by a phase represent the same physical state.

For comparison, we also derive the number of free parameters of a physical state associated with a generic (i.e., normal) PEPS. For such a PEPS, the rank-5 tensor T has $2d\chi^4$

free parameters. Now, because of the gauge freedom, J, Q can be chosen as arbitrary invertible matrices. Moreover, the total scaling factor of J, Q is irrelevant since it cancels with J^{-1}, Q^{-1}. Thus, each of J, Q has $2\chi^2 - 2$ free parameters. A general PEPS is not normalized, which corresponds to subtracting two additional free parameters from T. The number of free parameters is thus $2d\chi^4 - 4\chi^2 + 2$.

c. Solvable boundary tensors

Lastly, we consider the solvable boundary tensors associated with Eqs. (S18) and (S19). We explicitly analyze the left-boundary tensor; the rest is understood similarly. Here, we assume that the left boundary is described by a rank-4 tensor $L^{\mathrm{P}}_{\mathrm{brt}}$ as

$$(S23)$$

The boundary condition is solvable if L satisfies

$$(S24)$$

where the green ball depicts the doubled tensor $L^{\mathrm{P}}_{\mathrm{brt}} \otimes L^{*\mathrm{p}}_{\mathrm{brt}}$. One can immediately see that the boundary condition shown in Fig. (1b) of the main text is a special case of Eq. (S24) with Λ replaced by the identity and $L^{\mathrm{P}}_{\mathrm{brt}} = \delta_{\mathrm{p,r}}\delta_{\mathrm{t,b}}$.

3. Analytic expression of the transfer operator

Here we derive analytic expressions for the transfer operators of Eq. (13).

Due to the presence of the delta tensor in the plumbing tensor Eq. (10), folding results in bipartite spaces, but with each part carrying a copy of the other one in the computational basis. That is, contracting two delta tensors

$$= |00\rangle\langle 00| + |11\rangle\langle 11|, \qquad (S25)$$

results in a rank-2 projector. Thus, for convenience we only work in the subspace of its image and view $|00\rangle \to |0\rangle$, $|11\rangle \to |1\rangle$. Therefore, the green tensor in Eq. (13) (PEPS tensor after contracting the physical degrees) corresponds to a different plumbing tensor, obtained by squaring W element-wise as

$$\widetilde{W}_{\mathrm{lb,rt}}=\begin{pmatrix} \alpha & & & 1-\alpha \\ & \beta & 1-\beta & \\ & 1-\alpha & \alpha & \\ 1-\beta & & & \beta \end{pmatrix}. \qquad (S26)$$

For the latter use, we reorder $\widetilde{W}$ as

$$\widetilde{W}_{\mathrm{rt,lb}}=\begin{pmatrix} \alpha & & & 1-\beta \\ & \beta & 1-\alpha & \\ & 1-\beta & \alpha & \\ 1-\alpha & & & \beta \end{pmatrix}$$

$$=I_H \otimes \begin{pmatrix} \alpha & \\ & \beta \end{pmatrix}_V + \sigma_H^1 \otimes \begin{pmatrix} & 1-\beta \\ 1-\alpha & \end{pmatrix}_V. \quad (S27)$$

Here the last line suggests that we can interpret the tensor $\widetilde{W}$ as a joint operator acting on the product of two 2-dimensional spaces. We denote these spaces as horizontal, indexed with H, and vertical, indexed with V. The former corresponds to the indices l, r of the original $\widetilde{W}$ tensor and the latter corresponds to the b, t indices. We emphasize that, in the transfer opera-

tor given by Eq. (13), each tensor $\widetilde{W}$ at different positions i has its own horizontal space. But all tensors share a common vertical space since they are connected vertically. The transfer operator with $\phi' = \phi$ thus can be expressed as

$$\mathbb{T}_\phi^\phi = \mathrm{Tr}_V(\prod_i^M \widetilde{W}_i) \quad (S28)$$

with M the number of sites in the transfer operator. Without loss of generality, we assume M to be even. Now the transfer operator acts on a product of M horizontal spaces. Substituting Eq. (S27) into Eq. (S28) we directly see that $\mathbb{T}$ only consists of Identity and σ^1 operators. Moreover, due to the trace in Eq. (S28), $\mathbb{T}$ must include an even number of σ^1. After some algebraic calculations, we can obtain the expression

$$\mathbb{T}_\phi^\phi = I(\alpha^M + \beta^M) + \sum_{1 \le i < j \le M} \sigma_i^1 \sigma_j^1 (1-\alpha)(1-\beta)(\beta^{j-i-1}\alpha^{M+i-j-1} + \alpha^{j-i-1}\beta^{M+i-j-1})$$

$$+ \sum_{1 \le i < j < k < n \le M} \sigma_i^1 \sigma_j^1 \sigma_k^1 \sigma_n^1 (1-\alpha)^2(1-\beta)^2(\beta^{j-i+n-k-2}\alpha^{M+i-n+k-j-2} + \alpha^{j-i+n-k-2}\beta^{M+i-n+k-j-2}) + \cdots$$

$$+ 2\prod_{i=1}^M \sigma_i^1 (1-\alpha)^{M/2}(1-\beta)^{M/2} \quad (S29)$$

where $\cdots$ denotes terms with a larger (even) number of σ^1 matrices. Since Eq. (S29) is frustration-free and each factor is non-negative, we immediately see that there are two degenerate leading eigenvectors $|\psi_+\rangle = \otimes_i^M |+\rangle_i$, $|\psi_-\rangle = \otimes_i^M |-\rangle_i$. Here $|+\rangle = \frac{|0\rangle+|1\rangle}{\sqrt{2}}$, $|-\rangle = \frac{|0\rangle-|1\rangle}{\sqrt{2}}$ are the eigenvectors of σ^1. The linear combinations of these two vectors $\frac{|\psi_+\rangle+|\psi_-\rangle}{\sqrt{2}}$, $\frac{|\psi_+\rangle-|\psi_-\rangle}{\sqrt{2}}$ have even and odd parity, corresponding to $\mathbb{T}_{e\phi}^{e\phi}$, $\mathbb{T}_{o\phi}^{o\phi}$, respectively. Thus, $\lambda_{e\phi}^{e\phi} = \lambda_{o\phi}^{o\phi}$ always holds.

As long as we are not at the GHZ-points, where $\alpha = 1$ or $\beta = 1$ or $\alpha = \beta = 0$, each coefficient in Eq. (S29) is strictly positive. Any other state not spanned by $|\psi_+\rangle$ and $|\psi_-\rangle$ must

violate some terms in Eq. (S29) and thus decrease the leading eigenvalue. Therefore, the leading eigenvalue of $\mathbb{T}$ is at most 2-fold degenerate, each corresponding to one of the blocks $\mathbb{T}_{e\phi}^{e\phi}$, $\mathbb{T}_{o\phi}^{o\phi}$ separately.

If $\phi' = \phi + \pi$, the transfer operator is given by

$$\mathbb{T}_\phi^{\phi+\pi} = \mathrm{Tr}_V(\prod_i^M \widetilde{W}_i \sigma_V^3). \quad (S30)$$

After reasoning as above, the expression is

$$\mathbb{T}_\phi^{\phi+\pi} = I(\alpha^M - \beta^M) + \sum_{1 \le i < j \le M} \sigma_i^1 \sigma_j^1 (1-\alpha)(1-\beta)(\beta^{j-i-1}\alpha^{M+i-j-1} - \alpha^{j-i-1}\beta^{M+i-j-1})$$

$$+ \sum_{1 \le i < j < k < n \le M} \sigma_i^1 \sigma_j^1 \sigma_k^1 \sigma_n^1 (1-\alpha)^2(1-\beta)^2(\beta^{j-i+n-k-2}\alpha^{M+i-n+k-j-2} - \alpha^{j-i+n-k-2}\beta^{M+i-n+k-j-2}) + \cdots,$$

$$(S31)$$

which has a similar form as Eq. (S29) but with some coefficients changed from positive to negative. Thus, as long as we are not at the GHZ-points, the leading eigenvalue of Eq. (S31) must be lower than that of Eq. (S29). Since it still

has the symmetry $\otimes_i^M \sigma_i^3$, each eigenvalue is at least twice degenerate, one corresponds to $\mathbb{T}_{e\phi}^{e\phi+\pi}$ and the other to $\mathbb{T}_{o\phi}^{o\phi+\pi}$. Thus, we proved that as long as we are not at the GHZ-points,

$|\lambda_{\mathrm{e}\phi}^{\mathrm{e}\phi}| = |\lambda_{\mathrm{o}\phi}^{\mathrm{o}\phi}| > |\lambda_{\mathrm{e}\phi}^{\mathrm{e}\phi+\pi}| = |\lambda_{\mathrm{o}\phi}^{\mathrm{o}\phi+\phi}|$ and the blocks with the largest eigenvalues $\mathbb{T}_{\mathrm{e}\phi}^{\mathrm{e}\phi}, \mathbb{T}_{\mathrm{o}\phi}^{\mathrm{o}\phi}$ are nondegenerate. This implies that those states are in the same topological order as the toric code.

We illustrate the above ideas with two examples. The first example is $\beta = 1 - \alpha$. In this case, with a straightforward calculation, Eq. (S29) can be rewritten as

$$\mathbb{T}_\phi^\phi = \prod_i^{M-1} \left(\alpha I + (1-\alpha)\sigma_i^1 \sigma_{i+1}^1\right) \left(\alpha I + (1-\alpha)\sigma_M^1 \sigma_1^1\right). \tag{S32}$$

This transfer matrix has the leading eigenvalue 1 for eigenvectors $|\psi_+\rangle, |\psi_-\rangle$ as the only leading eigenvectors. The second leading eigenvalue is $(1-2\alpha)^2$ with the eigenvectors obtained by replacing one $|+\rangle$ ($|-\rangle$) from $|\psi_+\rangle$ ($|\psi_-\rangle$) with $|-\rangle$ ($|+\rangle$). As $\alpha \to 0$, the gap closes as 4α. Similarly, Eq. (S31) simplifies to

$$\mathbb{T}_\phi^{\phi+\pi} = \prod_i^{M-1} \left(\alpha I + (1-\alpha)\sigma_i^1 \sigma_{i+1}^1\right) \left(\alpha I - (1-\alpha)\sigma_M^1 \sigma_1^1\right). \tag{S33}$$

The absolute value of its leading eigenvalue is $|1 - 2\alpha|$ which is always smaller than 1 as long as $\alpha \neq 0, 1$.

The second example is $\beta = \alpha$ where, after straightforward calculations, Eq. (S29) can be rewritten as

$$\mathbb{T}_\phi^\phi = \prod_i^M \left(\alpha I + (1-\alpha)\sigma_i^1\right) + \prod_i^M \left(\alpha I - (1-\alpha)\sigma_i^1\right). \tag{S34}$$

In the above equation, the sum of the two terms ensures the symmetry $\otimes_i^M \sigma_i^3$ thus only terms with an even number of σ^1 can survive in the final result. This transfer operator has the leading eigenvalue $1 + (2\alpha - 1)^M$. The absolute value of the second one is $|2\alpha - 1| + |2\alpha - 1|^{M-1}$. The corresponding eigenvectors are the same as in the first example. As long as $\alpha \neq 0, 1$, the gap does not close. When $\alpha \to 0$, the gap closes as $4(M - 1)\alpha^2$. On the other hand, Eq. (S31) vanishes

$$\mathbb{T}_\phi^{\phi+\pi} = 0. \tag{S35}$$

4. Parent Hamiltonian

In this subsection, we discuss the parent Hamiltonian of the DI-PEPS constructed from the plumbing tensor Eq. (12) with $\alpha, \beta \in (0, 1)$. The special point $\alpha = \beta = 1/2$ corresponds to the toric code $|\mathrm{TC}\rangle$, which has the parent Hamiltonian

$$H = \sum_v \mathcal{A}_v + \sum_p \mathcal{B}_p, \tag{S36}$$

where $\mathcal{A}_v = I - \prod_{i \in v} \sigma_i^3$ and $\mathcal{B}_p = I - \prod_{i \in p} \sigma_i^1$ are four-body projectors constructed from the products of Pauli operators around each vertex v and plaquette p, respectively. Recall that the physical spins are at the edges of the lattice. The state

associated with general α and β can be obtained from the toric code by the local transformation up to a normalization factor as

$$|\psi\rangle = \prod_v \mathcal{U}_v |\mathrm{TC}\rangle, \tag{S37}$$

where $\mathcal{U}_v = \exp\{h_{\mathrm{b}}\sigma_{\mathrm{b}}^3 + h_{\mathrm{t}}\sigma_{\mathrm{t}}^3 + h_{\mathrm{bt}}\sigma_{\mathrm{b}}^3\sigma_{\mathrm{t}}^3\}$ are two-body operators acting vertically on each vertex. Here, the labels b and t represent the bottom and top edge of a vertex and $h_{\mathrm{b}} = \frac{1}{8}\ln\left(\frac{(\alpha-1)\alpha}{(\beta-1)\beta}\right)$, $h_{\mathrm{t}} = \frac{1}{8}\log\left(\frac{\alpha(\beta-1)}{(\alpha-1)\beta}\right)$, $h_{\mathrm{bt}} = \frac{1}{8}\log\left(\frac{\alpha\beta}{(\alpha-1)(\beta-1)}\right)$. The state $|\psi\rangle$ is therefore annihilated by

$$\widetilde{\mathcal{A}}_v = \prod_{v'} \mathcal{U}_{v'} \mathcal{A}_v \prod_{v'} \mathcal{U}_{v'}^{-1} = \mathcal{A}_v, \tag{S38}$$

$$\widetilde{\mathcal{B}}_p = \prod_{v'} \mathcal{U}_{v'} \mathcal{B}_p \prod_{v'} \mathcal{U}_{v'}^{-1}, \tag{S39}$$

where in the first equation we use the fact that $\mathcal{A}$ and $\mathcal{U}$ only consist of σ^3 and thus commute with each other. The corresponding parent Hamiltonian can be chosen as

$$\widetilde{H} = \sum_v \widetilde{\mathcal{A}}_v^\dagger \widetilde{\mathcal{A}}_v + \sum_p \widetilde{\mathcal{B}}_p^\dagger \widetilde{\mathcal{B}}_p. \tag{S40}$$

Note that in Eq. (S39), only the terms associated with the vertices which sit on the corner of the plaquette p contribute to $\widetilde{\mathcal{B}}_p$, as shown below

$$\tag{S41}$$
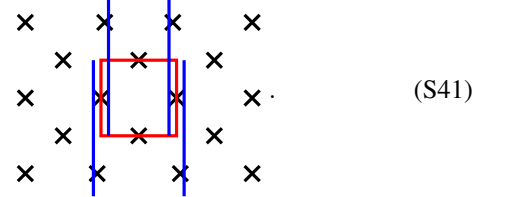
Here the red line denotes one plaquete operator $\mathcal{B}_p$, and the blue lines denote the four $\mathcal{U}_v$ which contribute in Eq. (S39). The crosses represent the physical spins, which are at the edge of the lattice. From this, we can see that $\widetilde{\mathcal{B}}_p$ is at most an 8-body operator. Since $\widetilde{\mathcal{A}}_v = \mathcal{A}_v$ is a 4-body operator, the parent Hamiltonian of the example Eq. (12) is at most 8-local. This can be compared to a general "plumbing" PEPS describing a eight-vertex model, where the parent Hamiltonian is 12-local [40].

For the special points where $\beta = 1 - \alpha$, we found that $h_{\mathrm{bt}} = 0$, thus $\mathcal{U}_v$ is decomposed to a product of two single-site operators. As can be seen in Eq. (S39), $\widetilde{\mathcal{B}}_p$ has the same locality as $\mathcal{B}_p$. Therefore, the parent Hamiltonians for those states are at most four-local.

5. Explicit form of W tensor

Here we report the general expression for a plumbing tensor to be a DI-PEPS. To this end, the explicit form of W tensor

can be obtained by directly substituting Eq. (10) to Eqs. (2) and (4). The parametrization of the resulting W tensor can be written as

$$W_{\text{lb,rt}} = \begin{pmatrix} \cos\alpha\cos\theta_1 e^{i\phi_1} & \cos\alpha\sin\theta_1 e^{i\phi_2} & \sin\alpha\sin\theta_2 e^{i\phi_3} & \sin\alpha\cos\theta_2 e^{i\phi_4} \\ \cos\beta\sin\theta_5 e^{i\phi_9} & \cos\beta\cos\theta_5 e^{i\phi_{10}} & \sin\beta\cos\theta_6 e^{i\phi_{11}} & \sin\beta\sin\theta_6 e^{i\phi_{12}} \\ \sin\alpha\sin\theta_3 e^{i\phi_5} & \sin\alpha\cos\theta_3 e^{i\phi_6} & \cos\alpha\cos\theta_4 e^{i\phi_7} & \cos\alpha\sin\theta_4 e^{i\phi_8} \\ \sin\beta\cos\theta_7 e^{i\phi_{13}} & \sin\beta\sin\theta_7 e^{i\phi_{14}} & \cos\beta\sin\theta_8 e^{i\phi_{15}} & \cos\beta\cos\theta_8 e^{i\phi_{16}} \end{pmatrix}. \tag{S42}$$

with all the angle variables take values in $[0, 2\pi)$. Note that the toric code corresponds to a special choice of the parameters $\theta_i = \phi_j = 0$ for all $i \in \{1, \cdots, 8\}, j \in \{1, \cdots, 16\}$ and $\alpha = \beta = \frac{\pi}{4}$.